Journal of Applied Electrochemistry **30**: 1335–1343, 2000.

LES of turbulent channel flow of a binary electrolyte[†]

F. GURNIKI[1], K. FUKAGATA[1,3], S. ZAHRAI[2] and F.H. BARK[1]
[1]*FaxénLaboratoriet, Royal Institute of Technology, Stockholm, S-10044 Sweden*
[2]*ABB, Corporate Research, S-72178 Västerås, Sweden*
[3]*Department of Quantum Engineering and Systems Science, University of Tokyo, 7-3-1 Hongo, Bunkyo-ku, Tokyo 113, Japan*

Received 26 July 1999; accepted in revised form 23 December 1999

Key words: Butler–Volmer, forced convection, high Schmidt number, large eddy simulation, near-wall region

Abstract

The turbulent diffusion boundary layer in a binary electrolyte was considered at Schmidt numbers of 1, 10 and 100 and exchange current densities between 10^{-4} A m^{-2} and 10^{-2} A m^{-2}. A numerical scheme was developed for efficient investigation of the dynamics by means of large eddy simulations. The methodology was examined by detailed comparisons with documented data from earlier large eddy and direct numerical simulations and good agreement was found. Application of the methodology to electrochemical mass transfer indicated that the exchange current density seems to have negligible effect on the mean concentration profile but it influences the structure of the fluctuating field in a visible manner.

List of symbols

c	concentration of a species
c_1	concentration of the metal ion
c_2	concentration of the anion
C^*	characteristic concentration, $-\frac{D}{u_\tau}\left(\frac{\partial \bar{c}}{\partial y}\right)_{\text{wall}}$
$\mathscr{C}$	subgrid-scale constant
$\mathscr{C}_o$	reference value for concentration at equilibrium
D	passive scalar molecular diffusivity (m^2 s^{-1}). For reduced concentration, D is a function of the molecular diffusivities for cation and anion species
E_c	eddy diffusivity, $-\overline{vc}\left(\frac{\mathrm{d}\bar{c}}{\mathrm{d}y}\right)^{-1}$ (m^2 s^{-1})
F	faradaic constant (96 485 C mol^{-1})
i_o	exchange current density due to mass transport (A m^{-2})
$\mathscr{J}_{\text{wall}}$	constant mass flux at the wall
$\mathscr{J}_o$	constant in the Butler–Volmer-like boundary condition $i_o/2FD_1Re_\tau$
$\mathscr{K}_o$	constant in the Butler–Volmer-like boundary condition $i_o/2FD_1\mathscr{C}_oRe_\tau$
l^*	viscous length scale v/u_τ (m)
$\mathscr{L}_j$	effective mixing length for subgrid eddy transport in direction j $\left((\Delta x_1^M \Delta x_2^M \Delta x_3^M)^{1/9}\ (\Delta x_j^M)^{2/3}\right)$
N_i	number of nodes of the mesh in the i-direction
p	pressure (N m^{-2})
Pr	Prandtl number v/α
Pr_t	turbulent Prandtl number v_t/α_t
r_z	streak half-spacing in the spanwise direction (m)
Re_τ	turbulent Reynolds number $u_\tau\delta/v$
s_{ij}	rate of strain $\left(\frac{\partial u_i}{\partial x_j}+\frac{\partial u_j}{\partial x_i}\right)$ (s^{-1})
Sc	Schmidt number v/D
Sc_t	turbulent Schmidt number v_t/D_t
Δs_i^M	area of surface normal to i-direction of the cell centered in $\mathbf{x}^M$ $\left(\Delta x_j^M \Delta x_k^M\right)$
t	time (s)
u_τ	friction velocity, $\sqrt{\frac{\tau_w}{\rho}}$ (m s^{-1})
u	x-component of the velocity vector (m s^{-1})
Δv^M	volume of the cell centred in $\mathbf{x}^M$ $\left(\Delta x_1^M \Delta x_2^M \Delta x_3^M\right)$
v	y-component of the velocity vector (m s^{-1})
w	z-component of the velocity vector (m s^{-1})
Δx_i^M	side length in the i-direction of the cell centred in $\mathbf{x}^M$ (m)
Δx	distance between two nodes of the grid in the x-direction (m)
Δy	distance between two nodes of the grid in the y-direction (m)
Δz	distance between two nodes of the grid in the z-direction (m)
z_1	charge number of the metal ion
z_2	charge number of the anion

Greek symbols

α	heat molecular diffusivity (m^2 s^{-1})
δ	half-width of the channel in the y-direction (m)

[†] Dedicated to the memory of Daniel Simonsson

δ_h	hydrodynamic boundary layer (m)
δ_c	diffusive boundary layer (m)
λ_i	periodicity length in the i-direction (m)
μ	dynamic viscosity of solution (kg m^{-1} s^{-1})
v	kinematic viscosity, μ/ρ (m^2 s^{-1})
ρ	fluid density (kg m^{-3})
τ_w	shear stress at the wall $\left(\mu\frac{\partial u}{\partial y}\right)_{\text{wall}}$ (kg m s^{-2})
τ_{ij}	stress tensor μs_{ij} (kg m s^{-2})

Subscripts

$\mathbf{g}$	A vector
$(\cdots)^M$	value $(\cdots)$ at the centre of the numerical cell $\mathbf{x}^M$
$(\cdots)^{(\pm j)M}$	considered filtered quantity evaluated on cell surface whose normal direction is j
$(\cdots)_{\max}$	maximum of the considered quantity
$(\cdots)_{\min}$	minimum of the considered quantity
$(\cdots)_{\text{rms}}$	RMS intensity of the considered quantity
$(\cdots)_t$	contribution from turbulence
$(\cdots)_{\text{wall}}$	value at the wall
$(\cdots)_x$	x-direction
$(\cdots)_y$	y-direction
$(\cdots)_z$	z-direction
$(\cdots)_1$	a value referred to the metallic ionic species, except when specified differently in the text
$(\cdots)_2$	a value referred to the nonmetallic ionic species, except when specified differently in the text
$\underline{(\cdots)}$	instantaneous value of $(\cdots)$
$\overline{(\cdots)}$	average value of $(\cdots)$ on time, except when specified differently in the text
$(\cdots)' = (\cdots) - \overline{(\cdots)}$	fluctuation with time of $(\cdots)$
$(\cdots)^+$	value made dimensionless with the wall parameters

1. Introduction

Numerical simulations of turbulent flows for industrial use are usually made by considering average fields. In such simulations, influence of turbulent fluctuations on the transport of different quantities must be modelled. Models are usually constructed based on information on the statistical structure of the flow. Making use of experimental data is a usual approach for development and verification of models.

Levich [1], based on the analogy with laminar boundary layer, proposed that in a turbulent boundary layer the thickness of the diffusion layer, δ_c, would be of the order of magnitude of $\delta_h \times Sc^{-1/3}$. It has been verified experimentally in different studies, for example by Lin et al. [2]. The high value of Schmidt number appearing in most of the practical applications is one of the important factors resulting in thin diffusion boundary layer, and making experimental investigation of flows with mass transfer problematic.

Unfortunately, although electrochemical systems seem to be suitable for experimental investigations, see e.g. [3], the measured data are usually in the form of integrated quantities rather than detailed information on the structure of the flow. As examples, Fouad et al. [4] and Newman [5] studied mass transfer in electrochemical systems and reported global information on the process such as the total cell potential drop, electrical current and global density variation of ionic species. As a result, other tools must be used to provide detailed data on the structure of the flow.

With increasing improvement in digital computers and computational methods, simulation can be used as an alternative to physical experiments. Study of turbulent channel flow, for example, has played an important role in modelling turbulence, in particular in the vicinity of a rigid wall. A pure numerical solution of the mathematical equations without a model is usually refered to as direct numerical simulation. Clearly, the advantage is that no models are involved at the cost of being limited to low Reynolds numbers. An alternative route is to use large eddy simulations, where only small eddies which have a more universal behaviour are modelled. Using large eddy simulations, higher Reynolds number can be studied.

In earlier studies, boundary conditions for the passive scalar were such that direct use of presented data for modelling of mass transfer at the electrode in an electrochemical system were not possible. The goal of the present study is to provide detailed information about the statistical structure of a turbulent boundary layer with mass transfer using boundary conditions of interest for electrochemical systems. Statistical data presenting the structure of the boundary layer are to be obtained by performing large eddy simulations. The hydrodynamic part of the computation performed by Zahrai et al. [6] is completed in the present study to treat the mass conservation equation.

2. Formulation of the problem

In this study turbulent flow of a binary electrolyte outside the double layers in an infinitely large cell is considered. The electrodes are assumed to be at a distance of 2δ and the flow is driven by a constant pressure gradient, strong enough to make gravitational effects negligible. The coordinate system is chosen so that the electrodes are located at $y = \pm\delta$. The electrical neutrality of the electrolyte can be expressed as $z_1c_1 + z_2c_2 = 0$, where c_i and z_i denote the concentration and the charge number of species i, respectively. The

transport equations for the mass in a binary electrolyte can be reduced to one single diffusion-convection equation for a concentration field defined by $c = z_1 c_1 = -z_2 c_2$. It can easily be shown that the charge neutrality will then be identically satisfied.

Under the above conditions, the flow can be described by the Navier–Stokes equations for an incompressible fluid, the law of conservation of mass for a fluid at constant density and a transport equation for the reduced concentration field. Using u_τ, the friction velocity, as the characteristic velocity scale, $l^* = \nu/u_\tau$, the typical length scale in wall units, the continuity and Navier–Stokes equations can be written for the instantaneous velocity vector as

$$\nabla^+ \cdot \mathbf{u}^+ = 0 \tag{1}$$

and

$$\frac{\partial \mathbf{u}^+}{\partial t^+} + (\mathbf{u}^+ \cdot \nabla^+)\mathbf{u}^+ = -\nabla^+ p^+ + \Delta^+ \mathbf{u}^+ \tag{2}$$

where $\mathbf{u}$ denotes the instantaneous velocity field and p is the instantaneous pressure field and is nondimensionalized by ρu_τ^2. The transport equation for the reduced instantaneous concentration field, using the above scales, can be written as

$$\frac{\partial c^+}{\partial t^+} + (\mathbf{u}^+ \cdot \nabla^+)c^+ = \frac{1}{Sc}\Delta^+ c^+ \tag{3}$$

where Sc is the Schmidt number. The concentration field can be made dimensionless by using the mass flux at the wall, i.e. $C^* = -\frac{D}{u_\tau}\left(\frac{\partial \bar{c}}{\partial y}\right)_{\text{wall}}$, where $\bar{c}$ corresponds to the averaged value of the instantaneous concentration. All quantities are thus scaled in wall units; therefore the superscript '+' will be dropped throughout the remainder of this paper. Nevertheless, for more clarity, the superscript can be maintained in the captions of the Figures. For the hydrodynamic equations, the no-slip condition is used at the electrodes. Note that the nondimensional half-channel width will be equal to Re_τ in the wall units. For the concentration field different boundary conditions are considered. As a first step, in order to make comparisons with earlier numerical and experimental investigations, the case of mass transfer when the concentration is set to a given value at the wall is considered, that is,

$$c(x, \pm Re_\tau, z, t) = \pm c_{\text{wall}} \tag{4}$$

For electrochemical systems, other boundary conditions are also of interest. Here, two simplified conditions are used for modelling the mass flux from the electrodes:

$$\frac{\partial c}{\partial y}(x, \pm Re_\tau, z, t) = \pm \mathscr{J}_{\text{wall}} \tag{5}$$

that is, the flux is given at the electrodes, and finally a boundary condition which allows fluctuations of the flux with the value of the concentration at the electrodes,

$$\frac{\partial c}{\partial y}(x, \pm Re_\tau, z, t) = \pm \mathscr{K}_{\text{o}}[c(x, \pm Re_\tau, z, t) - \mathscr{C}_{\text{o}}] \tag{6}$$

In the above relations, $\mathscr{C}_{\text{o}}$, $\mathscr{K}_{\text{o}}$ and $\mathscr{J}_{\text{wall}}$ are given constants. The form of the boundary condition in Equation 6 comes directly from the first term in a Taylor expansion of the Butler–Volmer mass transfer law (e.g., see [7]). $\mathscr{K}_{\text{o}}$ is proportional to the exchange current density of the chemical reaction at the wall and is equal to

$$\mathscr{K}_{\text{o}} = \frac{i_{\text{o}}}{2FD_1 \mathscr{C}_{\text{o}} Re_\tau} \tag{7}$$

where i_{o} is the exchange current density, F is the faradaic constant, D_1 is the salt diffusivity constant for the metallic ionic species of the binary electrolyte, and $\mathscr{C}_{\text{o}}$ a reference value for the reduced concentration at equilibrium, which is the same as in the core of the channel. If an electrolyte with low electrical potential gradients is considered, the boundary condition (6) is a good approximation of the electrochemical mass transfer law at the electrodes. Experimentally, such a configuration can be obtained with an additional ion that does not take part of the chemical reactions and reduces the electrical resistance of the electrolyte considerably [5]. Equation 6 can also be written as

$$\frac{\partial c}{\partial y}(x, \pm Re_\tau, z, t) = \pm[\mathscr{K}_{\text{o}} \cdot c(x, \pm Re_\tau, z, t) - \mathscr{J}_{\text{o}}] \tag{8}$$

where $\mathscr{J}_{\text{o}} = i_{\text{o}}/2FD_1 Re_\tau$. In this form, it is clear that for low values of $\mathscr{K}_{\text{o}}$, this boundary condition approaches Equation 5. It is worth noting that the exposed boundary conditions above are linear and remain the same when considering the time-averaged values.

3. Numerical procedure

The methodology used for the fluid velocity field is taken from the earlier work on the simulation of turbulent channel flows by Zahrai et al. [6]. In this large eddy simulation, averaging over the volume of the computational cells is used as the filtering function. The subgrid model is an anisotropic version of the Smagorinsky eddy viscosity model. A rectangular computational cell, numbered M, has the width in the i-direction, Δx_i^M, the area of surface normal to i-direction, $\Delta s_i^M = \Delta x_j^M \Delta x_k^M$, and a volume size, $\Delta v^M = \Delta x_1^M \Delta x_2^M \Delta x_3^M$. The modelled Navier–Stokes equation (2) averaged over the volume using the cell M, which gives the dynamics of large eddies resolved on the given mesh, can be expressed as

$$\Delta v^M \frac{\partial \bar{u}_i^M}{\partial t} = \sum_{j=1}^{3} \Delta s_j^M \left[-\left(u_i^{(+j)M} u_j^{(+j)M} - u_i^{(-j)M} u_j^{(-j)M} \right) - \left(p^{(+j)M} - p^{(-j)M} \right) \delta_{ij} \right] + \sum_{j=1}^{3} \Delta s_j^M \left[+\left(\tau_{ij}^{(+j)M} - \tau_{ij}^{(-j)M} \right) + \frac{1}{\sqrt{2}} \mathscr{C}^2 \mathscr{L}_j^2 \times \left(\left| \bar{s}_{ij}^M \right|^{(+j)M} \cdot s_{ij}^{(+j)M} - \left| \bar{s}_{ij}^M \right|^{(-j)M} \cdot s_{ij}^{(-j)M} \right) \right] \quad (9)$$

where τ_{ij} is the resolved stress tensor, and s_{ij} the deformation tensor, $\left|\bar{s}_{ij}^M\right| = \left(\sqrt{\sum_{i=1}^{3}\sum_{j=1}^{3} \bar{s}_{ij}^{M^2}}\right)$, and $\mathscr{L}_j^2 = (\Delta x_1^M \Delta x_2^M \Delta x_3^M)^{2/9} (\Delta x_j^M)^{4/3}$. Considering an instantaneous function $f(\boldsymbol{x})$, $\bar{f}^M$ stands for the filtered version of f at the centre of cell M, whose volume is Δv^M. The superscript $(\pm j)M$ denotes that the considered filtered quantity is evaluated on the cell surface whose centre is the vector $\boldsymbol{x}^M \pm \frac{1}{2}\Delta x_j^M \boldsymbol{e}_j$ and whose normal direction is $\boldsymbol{e}_j$.

The above equation is not differenced but only filtered by integrating the Navier–Stokes equations on a cell volume. The transport through the cell surfaces due to fluctuations of smaller sizes than the size of the cell are modelled by a Smagorinsky-like subgrid viscosity. The modified Smagorinsky model has the property of vanishing in the regions where the resolution is good enough in an anisotropic manner. As a result, in the wall-region where the mesh size is chosen so that the details of the flow can be studied, the influence of the model becomes weak without explicit damping. The fine resolution of the flow near the wall eliminates the need of wall functions. The model constant $\mathscr{C}$ was set to 0.08, as suggested in [6]. The flow is driven by a body force, or by a pressure gradient constant in space and time. In other words, the pressure term is decomposed into a mean pressure gradient: that is, a given constant equal to 1 in wall units, and a fluctuating part which is to be solved together with the velocity field.

Similarly, the mass transport equation can be filtered at each cell M, which can differ from ones used for the velocity field. The turbulent Schmidt number, Sc_t, was set to 0.25, which may be a reasonable value, since the turbulent Prandtl number Pr_t, in the cases of large eddy simulation with heat transfer, is usually proposed to be between 1/2 and 1/3 (e.g., see [8]).

The computational domain is periodic in the streamwise and the spanwise directions with corresponding periodicity lengths, λ_x and λ_z. The distance between the channel walls is $2Re_\tau$. λ_x and λ_z are, respectively, $4 \times \pi \times Re_\tau$ and $2 \times \pi \times Re_\tau$, see Figure 1. Periodic boundary conditions are applied for the pressure fluctuations, the instantaneous velocity, and concentration in the streamwise and spanwise direction.

As a unique feature of this study, the use of different mesh systems for the fluid velocity field and the concentration field should be pointed out. Table 1 shows the characteristics of three meshes. The one denoted as mesh $1 \times 1 \times 1$ is used for the fluid velocity field. The meshes used for the concentration field are mesh $1 \times 2 \times 1$, and mesh $1 \times 6 \times 1$. The finest mesh, mesh $1 \times 6 \times 1$, was used for the the calculations performed at $Sc = 100$ only. The grids are uniform in the mean flow direction. They are stretched in the direction normal to the wall, with the finest spacing at the walls. According to Calmet et al. [9], at least three mesh points in the wall-normal direction are required within the diffusive sublayer, $y < 5/Sc^{1/3}$, to resolve the unlinear behavior near the wall. The mesh systems used in the study fulfill this requirement.

The initial profile in a cross section for the velocity was set parabolic. The mass transfer calculation was not added until the hydrodynamic simulation had reached statistically equilibrium state. The initial profile in a cross section for the reduced concentration was linear for the first calculation, at $Sc = 1$ and with a fixed value as the boundary condition at the walls. The calculations with other boundary conditions or higher Sc were initialized with the calculated concentration field obtained with the highest available Schmidt number. The calculated variables were considered to be at equilibrium when variation of the statistical properties in time were small.

4. Results

The flow is assumed to take place at Reynolds number of 180 based on the wall friction velocity and the

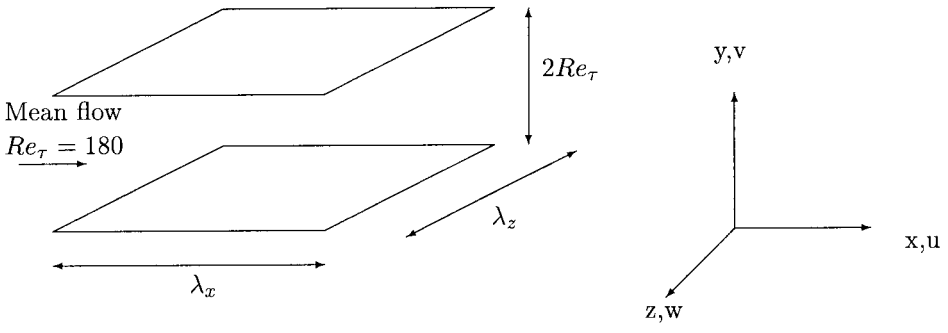

Fig. 1. Geometry of the cell and the chosen coordinate system.

Table 1. Mesh specification

	N_x	N_y	N_z	Δx	Δz	$\Delta y_{\min}$	$\Delta y_{\max}$
Mesh $1 \times 1 \times 1$	32	42	96	70.6858	11.781	1.4062	18.92
Mesh $1 \times 2 \times 1$	32	84	96	70.6858	11.781	0.7031	9.46
Mesh $1 \times 6 \times 1$	32	252	96	70.6858	11.781	0.2344	3.16

channel half width. The conditions of computation of the velocity field are exactly the same as those reported in [6]. The present study focuses on the mean concentration field, RMS intensities, the eddy diffusivity, and the structure of the instantaneous concentration field. Transport equations are solved for the concentration field at Schmidt number 1,10 and 100.

In Figure 2, the mean concentration profile in the direction normal to the walls is presented for $Sc = 1$. Good agreement is found with results from direct numerical simulations by Lyons et al. [10] and Papavassiliou et al. [11]. The methodology and subgrid-scale model used in the present study are consequently found to be accurate enough to model the turbulence mass transport on small scales. Figure 3 indicates similar variation of the mean concentration profile in the logarithmic diagram. With increasing y^+, the concentration profile exhibits a buffer layer character, followed by a logarithmic region. As shown on Figure 3, the concentration profile in the outer region fits well with the logarithmic law of $\bar{c}^+ = 3.6\ln(y^+) + 1.7$ after $y^+ = 30$. The constants of the logarithmic law found in the present study agree well with the mean profiles predicted by Lyons et al. [10] and Papavassiliou et al. [11].

Figures 2 and 3 also present the average concentration calculated with the Butler–Volmer-like boundary condition (6) and the three different values of $\mathscr{K}_o$. No influence of $\mathscr{K}_o$, or the exchange current density, can be observed on the mean concentration profiles.

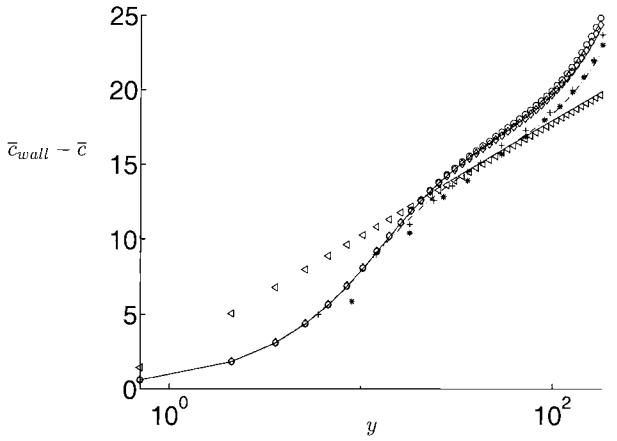

Fig. 3. Mean concentration at $Sc = 1$ in the normal direction to the walls and in the near-wall region. Key: (–·–) present study, $\tilde{c}_{\text{wall}} = \pm 1/C^*$; (– –) present study, $\left(\frac{\partial c}{\partial y}\right)_{\text{wall}} = \pm \mathscr{J}_{wall}$; (◇ ◇ ◇) present study, $\mathscr{K}_o = 1/Re_\tau$; (—) present study, $\mathscr{K}_o = 10/Re_\tau$; (○ ○ ○) present study, $\mathscr{K}_o = 100/Re_\tau$; (◁ ◁ ◁) $\bar{c}^+ = 3.6\ln(y^+) + 0.5$.

The RMS levels for the concentration field are calculated at Schmidt numbers and $\mathscr{K}_o$ mentioned above, and presented in Figure 4. Very good agreement is obtained with the results presented by Lyons et al. [10], performed with a fixed value of concentration set at the walls. Moreover, RMS levels computed with the boundary condition (6) and $\mathscr{K}_o = 10/Re_\tau$, have intermediary values between the two results obtained with $\mathscr{K}_o = 1/Re_\tau$ ($i_o = 10^{-4}$ A m^{-2}) and $\mathscr{K}_o = 100/Re_\tau$ ($i_o = 10^{-2}$ A m^{-2}). Therefore, at $Sc = 1$, RMS levels close to the wall are likely to be a monotonic function of $\mathscr{K}_o$, or i_o, and seem to decrease with increase in exchange current density.

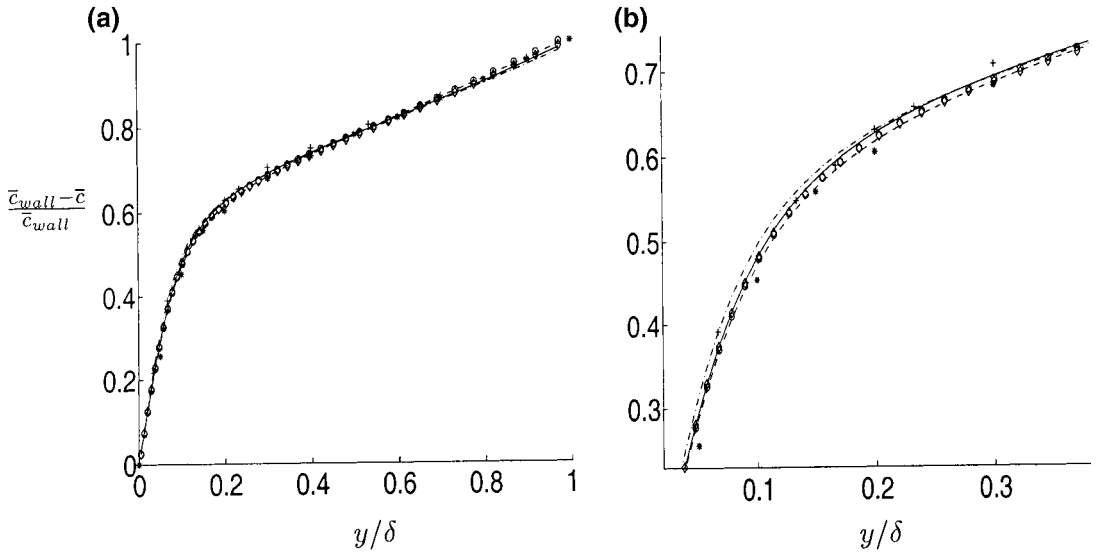

Fig. 2. Mean concentration at $Sc = 1$ in the normal direction to the walls. Key: (–·–) present study, LES, $Re_\tau = 180$, $c_{\text{wall}} = \pm 1/C^*$; (– –) present study, $\left(\frac{\partial c}{\partial y}\right)_{\text{wall}} = \pm \mathscr{J}_{\text{wall}}$; (◇ ◇ ◇) present study, $\mathscr{K}_o = 1/Re_\tau$; (—) present study, $\mathscr{K}_o = 10/Re_\tau$; (○ ○ ○) present study, $\mathscr{K}_o = 100/Re_\tau$; (∗ ∗ ∗) Lyons [10], DNS, $Re_\tau = 150$; (+ + +) Papavassiliou [11], DNS, $Re_\tau = 150$.

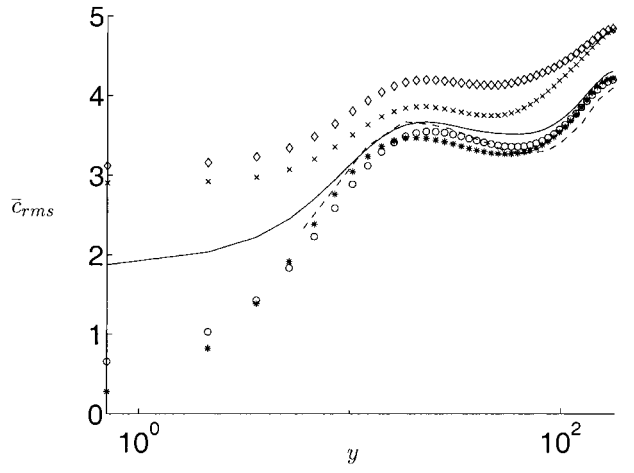

Fig. 4. RMS levels of the concentration field at $Sc = 1$ in the normal direction of the walls. Key: ($*\,*\,*$) present study, $c_{\text{wall}} = \pm 1/C^*$; ($\times\,\times\,\times$) present study, $\left(\frac{\partial c}{\partial y}\right)_{\text{wall}} = \pm \mathscr{J}_{\text{wall}}$; ($\diamond\,\diamond\,\diamond$) present study, $\mathscr{K}_{\text{o}} = 1/Re_\tau$; (—) present study, $\mathscr{K}_{\text{o}} = 10/Re_\tau$; ($\circ\,\circ\,\circ$) present study, $\mathscr{K}_{\text{o}} = 100/Re_\tau$; (– – –) Lyons [10].

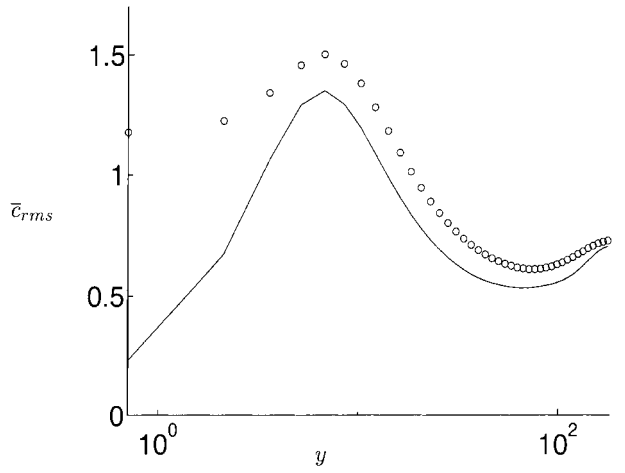

Fig. 5. RMS levels of the concentration field at $Sc = 10$ in the normal direction of the walls. Key: (—) present study, $c_{\text{wall}} = \pm 1/C^*$; ($\circ\,\circ\,\circ$) present study, $\left(\frac{\partial c}{\partial y}\right)_{\text{wall}} = \pm \mathscr{J}_{\text{wall}}$.

An issue of interest is the assymptotic behaviour of the Butler–Volmer-like, equation (6), with respect to variations of $\mathscr{K}_{\text{o}}$, defined in Equation 7. At high values of $\mathscr{K}_{\text{o}}$, or at high exchange current densities, the right hand side of Equation 6 becomes dominant. The system becomes sensitive to small variations of the concentration at the wall and tends to balance them fast. In the limiting case where $\mathscr{K}_{\text{o}}$ approaches infinity, Equation 6 becomes equivalent to Equation 4, that is, the system acts as one with a fixed value set for concentration at the wall. At low values of $\mathscr{K}_{\text{o}}$, the fluctuations of the concentration gradient at the wall are damped and the behaviour of Equation 6 becomes similar to a constant flux at the wall. As a result, the diffusion boundary layer simulated with the Butler–Volmer-like boundary condition (6) at a low exchange current density, is expected to have similar behaviour as that with a constant flux for the boundary condition, and at a high exchange current density, similar to the case with a fixed value at the walls. A comparison between profiles found with different values of $\mathscr{K}_{\text{o}}$ in Figure 4, confirms the proposed behavior. Figures 5 and 6 show RMS intensities calculated with Equations 4 and 5, at Schmidt numbers of 10 and 100, respectively. As expected, values predicted with a fixed value set at the walls, are lower than RMS intensities predicted with a constant flux. Similar behavior was predicted at $Sc = 1$. Since the above discussion does not account for values of Schmidt number, it is possible, at any Schmidt number, to draw conclusions about the effect of very low and very high exchange current densities on RMS intensities, on the basis of calculations made only with a fixed value and a constant flux set at the walls.

The mean eddy diffusivity, defined as $E_{\text{c}} = -\overline{vc}\left(\frac{\text{d}\bar{c}}{\text{d}y}\right)^{-1}$, is presented for different cases in Figures 7, 8 and 9. Figure 7 shows good agreement between the prediction of the present study, the prediction of Papavassiliou et al. [11], and the empirical profile proposed by

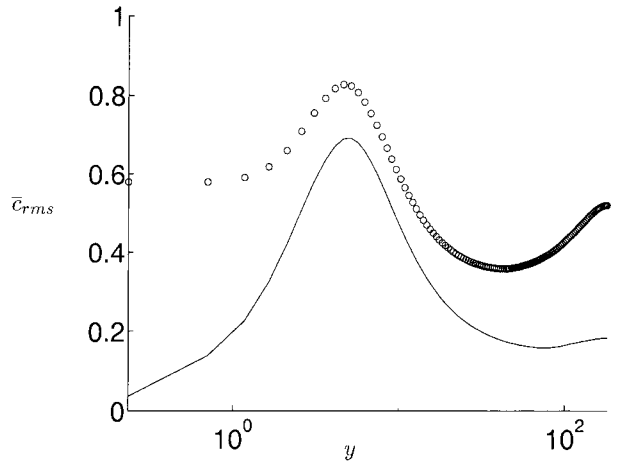

Fig. 6. RMS levels of the concentration field at $Sc = 100$ in the normal direction of the walls. Key: (—) present study, $c_{\text{wall}} = \pm 1/C^*$; ($\circ\,\circ\,\circ$) present study, $\left(\frac{\partial c}{\partial y}\right)_{\text{wall}} = \pm \mathscr{J}_{\text{wall}}$.

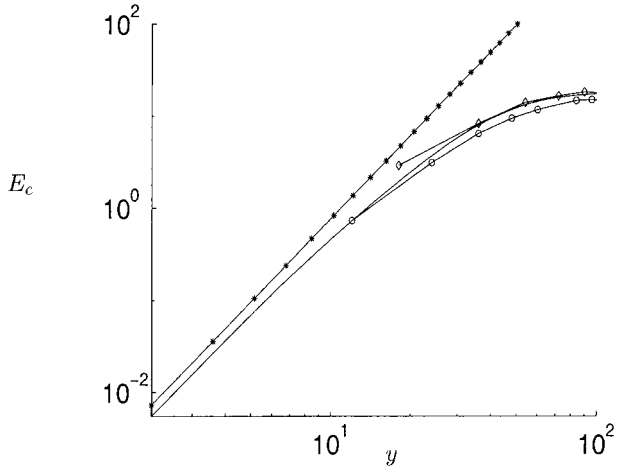

Fig. 7. Mean eddy diffusivity in the near-wall region at $Sc = 1$. Key: ($*\,*\,*$) $E_{\text{c}} = 0.000\,775\,y^3$ [11]; (—) present study, $c_{\text{wall}} = \pm 1/C^*$; ($\circ\,\circ\,\circ$) Papavassiliou [11]; ($\diamond\,\diamond\,\diamond$) Lyons [10].

Papavassiliou et al. [11]. Figures 8 and 9 indicate that the eddy diffusivity is not influenced by the values of $\mathscr{K}_o$, or the exchange current density i_o. The fact that the eddy-diffusivity is found to be independent of $\mathscr{K}_o$ can be related to the same observation for the mean concentration profile (see Figures 2 and 3).

Streamwise and wall-normal turbulent passive mass flux are presented in Figures 10 and 11. Good agreement is found with the direct numerical simulation of Kawamura et al. [12]. No data from previous results were available for comparison with the predictions of the present study at $Sc > 5$. The present study finds, as the last mentioned study, that the scalar fluctuations correlate more strongly with the streamwise velocity than with its normal-wall component. Figure 10 shows that the exchange current influences the range of strong correlation between the streamwise velocity and the scalar fluctuations. Inversely, no influence of the exchange current is noticed on the correlation between the wall-normal velocity and the scalar fluctuations (see Figure 11).

Iso-lines of the instantaneous concentration fluctuations for $Sc = 1$ in a $(x$–$z)$ section at $y^+ = 6.76$ are presented in Figure 12. The presence of well-known streaky structures elongated in the streamwise direction is clearly observed. Such structures are typical for turbulent flows in the viscous sublayer [13].

To compute the results in Figure 12, the Butler–Volmer-like law has been used. The influence of the exchange current on the streaks is studied, by comparing Figure 12(a), which presents a field computed with $\mathscr{K}_o = 10/Re_\tau$, and Figure 12(b) which corresponds to $\mathscr{K}_o = 100/Re_\tau$. Even if it is not possible here to give a

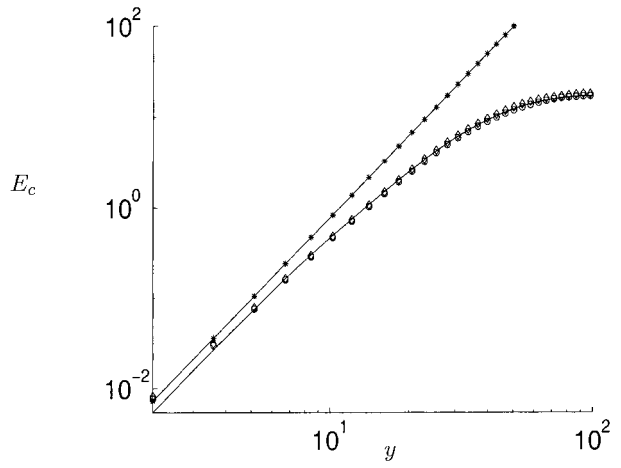

Fig. 8. Mean eddy diffusivity in the near-wall region at $Sc = 1$. Key: $(***)$ $E_c = 0.000\,775\,y^3$ [11]; (—) $c^+_{\text{wall}} = \pm 1/C^*$; $(\circ\circ\circ)$ $\left(\frac{\partial c}{\partial y}\right)_{\text{wall}} = \pm \mathscr{J}_{\text{wall}}$; $(\diamond\diamond\diamond)$ $\left(\frac{\partial c}{\partial y}\right)_{\text{wall}} = \pm\left(\frac{c_{\text{wall}}}{Re_\tau} - \mathscr{J}_o\right)$.

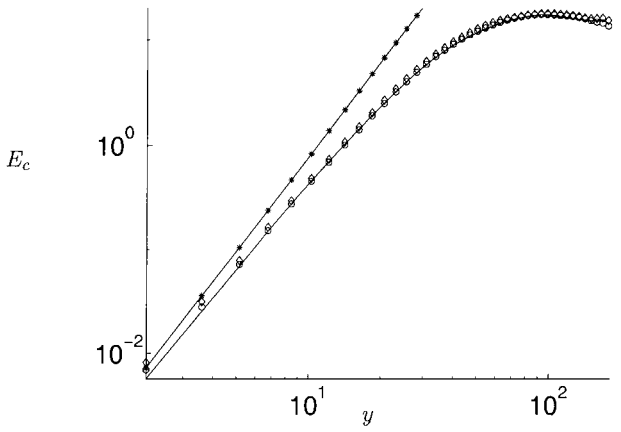

Fig. 9. Mean eddy diffusivity in the near-wall region at $Sc = 1$. Key: (—) $\mathscr{K}_o = 100/Re_\tau$; $(\circ\circ\circ)$ $\mathscr{K}_o = 10/Re_\tau$; $(\diamond\diamond\diamond)$ $\mathscr{K}_o = 1/Re_\tau$.

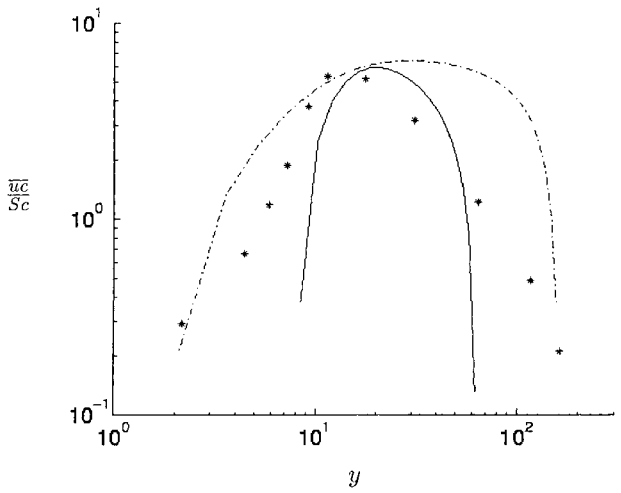

Fig. 10. At $Sc = 1$, the streamwise turbulent heat flux. Results computed with the Butler–Volmer-like boundary condition. Solid line, $\mathscr{K}_o = 10/Re_\tau$. Dashed lines, $\mathscr{K}_o = 100/Re_\tau$. Stars account for the numerical results of Kawamura et al. [12], with $Re_\tau = 180$ and $Sc = 1.5$.

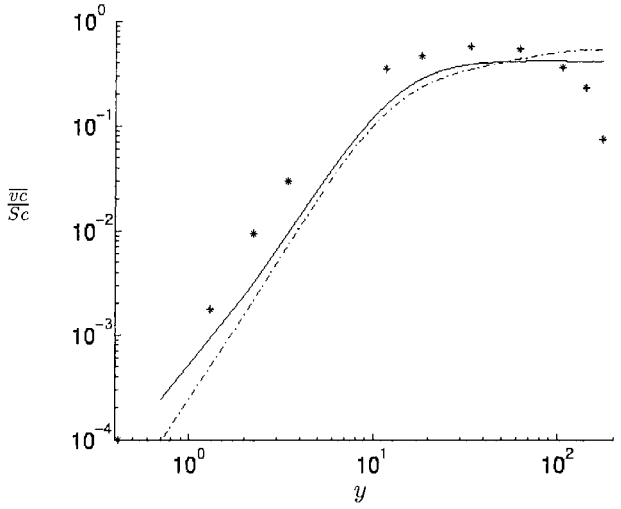

Fig. 11. At $Sc = 1$, the wall-normal turbulent heat flux. Results computed with the Butler–Volmer-like boundary condition. Solid line, $\mathscr{K}_o = 10/Re_\tau$. Dashed lines, $\mathscr{K}_o = 100/Re_\tau$. The stars account for the numerical results of Kawamura et al. [12], with $Re_\tau = 180$ and $Sc = 1.5$.

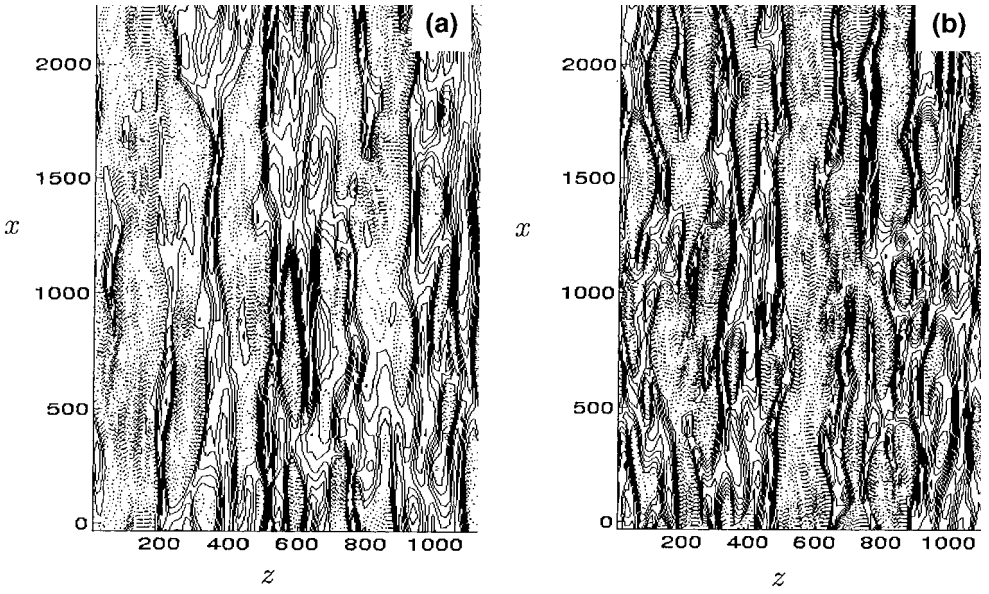

Fig. 12. At $Sc = 1$, snapshot contour plots of the concentration fluctuations in a $(x–z)$ plane at $y^+ = 6.76$. Results computed with the Butler–Volmer-like boundary condition. The increment in scalar is 0.02. Solid lines represent $0.0 \leq c' \leq c'_{max}$. Dashed lines $c'_{min} \leq c' \leq 0.0$. (a) $\mathscr{K}_o = 10/Re_\tau$. $c'_{min} = -0.323$, $c'_{max} = +0.21$. (b) $\mathscr{K}_o = 100/Re_\tau$. $c'_{min} = -0.457$, $c'_{max} = +0.186$.

clear quantitative approximation of the spacing, it seems that the spanwise spacing decreases with the increasing exchange current. This result is confirmed by the computation of the two-point spanwise correlation coefficients of the concentration fluctuations (see Figure 13). Considering the normal distance from the wall to the first local minimum of the spanwise correlation coefficient as the mean streak half-spacing, Calmet et al. found $r_z^+ = 100$. With the same method (at $Sc = 1$) the present study found, r_z^+ around 65 with an intermediate exchange current, and around 55 with a high exchange current (see Figure 13). These two results are in good agreement with the computed spacing found by Kline et al. [13].

At $Sc = 100$, the concentration fluctuations were plotted in the viscous sublayer in a section $(x–z)$ at $y^+ = 6.76/Sc^{1/3} = 1.17$ (see Figure 14). Again, the streaky structure of fluctuations are clearly observed.

Figure 15 presents the instantaneous concentration fluctuations in the logarithmic region at $y^+ = 54.1$. The streaky structures are no longer visible. Here, $\mathscr{K}_o$ is taken equal to 10 and 100 only. At these values, the

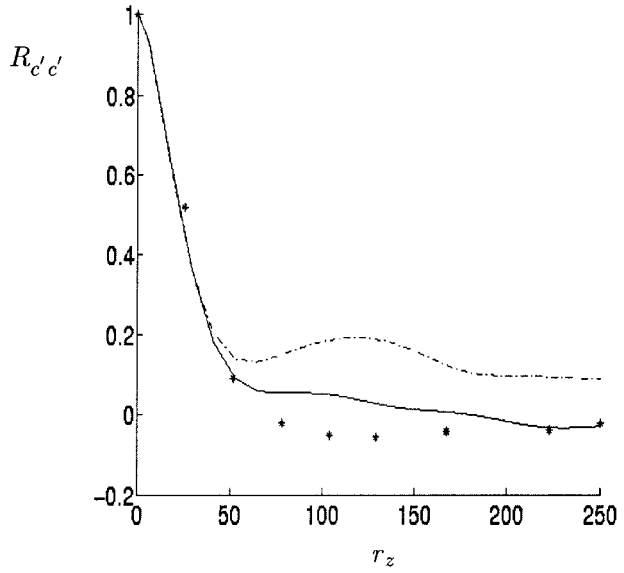

Fig. 13. At $Sc = 1$, spanwise two-point correlation coefficients at $y^+ = 6.76$. Results computed with the Butler–Volmer-like boundary condition. Solid line, $\mathscr{K}_o = 10/Re_\tau$. Dashed lines, $\mathscr{K}_o = 100/Re_\tau$. The stars account for the numerical results of Calmet et al. [9] at $y^+ = 1.7$, $Re_\tau = 640$, and a Dirichlet boundary condition at the walls.

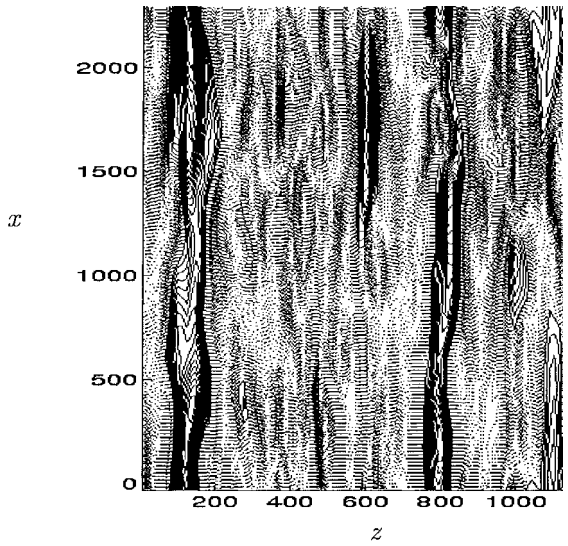

Fig. 14. At $Sc = 100$, snapshot contour plots of the concentration fluctuations in a $(x–z)$ plane at $y^+ = 1.17$. Results computed with a constant flux for concentration at the walls. Increment in scalar is 0.02. Solid lines represent $0.0 \leq c' \leq c'_{max}$. Dashed lines $c'_{min} \leq c' \leq 0.0$. $c'_{min} = -0.687$, $c'_{max} = 0.379$.

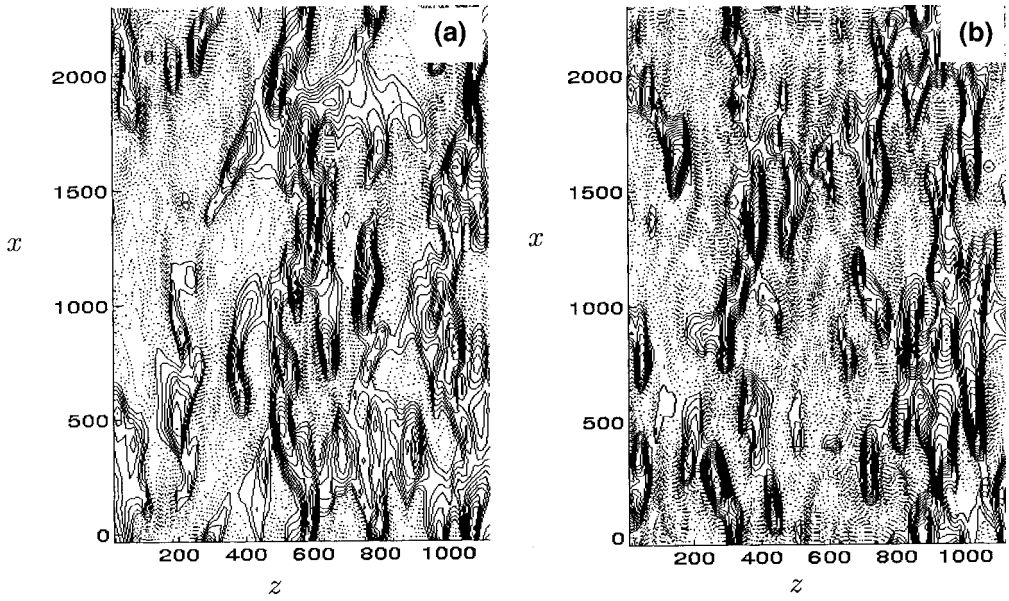

Fig. 15. At $Sc = 1$, snapshot contour plots of the concentration fluctuations in a (x–z) plane at $y^+ = 54.1$. Results computed with the Butler–Volmer-like boundary condition. Increment in scalar is 0.02. Solid lines represent $0.0 \leq c' \leq c'_{\max}$. Dashed lines $c'_{\min} \leq c' \leq 0.0$. (a) $\mathscr{K}_o = 10/Re_\tau$. $c'_{\min} = -0.43$, $c'_{\max} = +0.262$. (b) $\mathscr{K}_o = 100/Re_\tau$. $c'_{\min} = -0.575$, $c'_{\max} = +0.325$.

exchange current density has not influenced the wall-normal location of the streaky structures. This was expected, since the streaky structures are traditionally observed in the diffusive viscous sublayer [9]. But supplementary computations with different values of exchange current would allow confirmation of this result, and its extension to a larger range of exchange currents.

5. Conclusions

A model problem for studying the mechanisms of turbulent mass transfer in an electrochemical system by means of large eddy simulations is proposed. First, it was shown that the methodology was able to successfully reproduce documented literature results. Both mean profiles and fluctuations were predicted accurately. The influence of the exchange current density on the turbulent diffusion layer was investigated at Schmidt numbers of 1, 10 and 100. The studied range of the exchange current density was between $i_o = 10^{-4}$ A m^{-2} and $i_o = 10^{-2}$ A m^{-2}. Three different boundary conditions for the concentration field were used at the walls, i.e. a linearized Butler–Volmer-like condition, a given value and a given flux. At $Sc = 1$, the exchange current was shown to have no influence on the structure of the mean concentration, neither on the eddy diffusivity, nor on the wall-normal turbulent heat flux. However, the RMS intensities, the streamwise turbulent heat flux, and the lateral dimensions of turbulence structures in the near-wall region were influenced. The Butler–Volmer-like boundary condition predicts results close to those obtained with a given value at the wall if the exchange current density is high, and close to those obtained with a given flux if the exchange current density is low.

References

1. V.G. Levich, 'Physicochemical Hydrodynamics' (Prentice-Hall, Englewood Cliffs, NJ, 1962), p. 293.
2. C.S. Lin, R.W. Moulton and G.L. Putnam, *Ind. Eng. Chem.* **45** (1952) 636.
3. R.J. Goldstein, H.D. Chiang and D.L. Lee, *J. Fluid Mech.* **213** (1990) 111.
4. M.G. Fouad and N. Ibl, *Electrochim. Acta* **3** (1960) 233.
5. J.S. Newman, 'Electrochemical Systems', 2nd edn. (University of California, Berkeley Prentice Hall, Englewood Cliffs, NJ, 1991).
6. S. Zahrai, F.H. Bark and R.I. Karlsson, *Eur. J. Mech. B, Fluids* **14** (1995) 459.
7. F.H. Bark and F. Alavyoon, *J. Fluid Mech.* **290** (1995) 1.
8. Y. Miyake, 'Computational Fluid Dynamics', edited by M. Yasuhara and H. Daiguji, (University of Tokyo Press, Tokyo, 1992), Chapter 10, p. 223.
9. I. Calmet and J. Magnaudet, *Phys. Fluids* **9** (1997) 438.
10. S.L. Lyons, T.J. Hanratty and J.B. McLaughlin, *Int. J. Numer. Methods Fluids* **13** (1991) 999.
11. D.V. Papavassiliou and J. Thomas Hanratty, *Int. J. Heat Mass Transf.* **40** (1997) 1303.
12. H. Kawamura, K. Ohsaka, H. Abe and K. Yamamoto, *Int. J. Heat Fluid Flow* **19** (1998) 482.
13. S.J. Kline, W.C. Reynolds, F.A. Schraub and P.W. Runstadler, *J. Fluid Mech.* **30** (1967) 741.